Progress In Electromagnetics Research C, Vol. 173, 279–292, 2026

PIER C

(Received 24 April 2026, Accepted 24 August, Scheduled 18 September 2026)

A Compact PIN Diode-Based Independently Fed Frequency and Pattern Reconfigurable Hybrid Antenna Array for Wireless Applications

Yogesh S. Ghodake[1,*] and Shankar D. Nawale[2]

[1]*SKN Sinhgad College of Engineering, Korti, Pandharpur, India*
[2]*N. B. Navale Sinhagad College of Engineering, Kegaon, Solapur, India*

ABSTRACT: This paper proposes a compact, independently fed hybrid antenna array featuring reconfigurable frequency and radiation patterns for adaptive wireless applications, employing PIN diodes. The hybrid arrangement incorporates independently driven elements with diode-controlled current pathways to enable concurrent spectral and spatial tuning within a single structure. Frequency agility is achieved via PIN-diode switching configurations; five representative states are presented due to the similarity among the other responses, with resonant frequencies derived from the minima of the S-parameters. Multiband operation is demonstrated in simulation from 3.8 to 6.49 GHz and in measurement from 4.18 to 6.56 GHz; the mutual coupling suppression is achieved by an independently fed architecture, maintaining inter-port isolation better than 18–20 dB throughout the operating band, which signifies effective suppression of mutual coupling within the operating band. Radiation-pattern reconfigurability is achieved via PIN diode switching, yielding directional radiation-pattern reconfigurability through electronic switching via controlled redistribution of surface current. The design remains compact at $40 \times 44\,\text{mm}^2$ and uses only four PIN diodes, reducing switching complexity while preserving stable gain and radiation performance. Measured results show good agreement with simulations, validating the design's effectiveness. The proposed antenna provides a compact and low-complexity solution for adaptive sub-6 GHz wireless communication systems requiring simultaneous frequency and radiation-pattern reconfigurability.

1. INTRODUCTION

The rapid evolution of modern wireless communication systems has created a need for antennas that can dynamically adapt their spectral and spatial properties while remaining compact and low in hardware complexity. Fixed traditional antennas often cannot provide the multi-standard and wideband adaptive operation required, which increases system size and decreases flexibility. Frequency-tuneable and radiation-pattern-controllable antennas can solve this problem by integrating these functionalities in one structure. The fast advancement of wireless technologies demands frequency-agile, cognitive, and software-defined radio-frequency (RF) systems to ensure efficient use of spectrum, as well as power [1]. Such systems call for multifunctional antennas. Tuneable antenna architectures. Frequency reconfiguration is typically accomplished by modifying the electrical length of the radiating element through additional passive or active components. Desirable attributes of configurable antennas include tuneable operating frequency, radiation-pattern control, and polarization agility, all while maintaining a compact form factor. Reconfiguration is commonly realized by altering radiating elements, feed networks, or parasitic structures to achieve the desired operational flexibility [2]. Ideally, reconfiguration of a single antenna parameter should not degrade other performance metrics; however, achieving this in practice is challenging. Nonetheless, integrating multiple reconfiguration capabilities within a single antenna can markedly enhance system performance and adaptability [3–5]. Several adaptable antenna designs have been reported in the literature. A multiband antenna operating at GSM and Long-Term Evolution lower bands is described, though with reduced efficiency [6]. A Microelectromechanical System (MEMS) switch-based reconfigurable patch antenna with ground-plane modification for quad-band operation is discussed in [7]. A fork-shaped antenna employing four PIN diodes achieves both frequency and pattern reconfigurability in [8]. An ultra-wideband antenna incorporating a defective-ground-structure (DGS) and PIN diodes for multiband frequency reconfiguration is demonstrated in [9]. A frequency-reconfigurable antenna targeting fifth-generation applications is proposed in [10]. A compact 2×2 Vivaldi antenna with a return loss of -9 dB is presented in [11]. A complex frequency-agility for cognitive radio applications supporting 3.25 GHz and 4.1 GHz is reported [12]. In [13], another study used twelve SMP1345-079LF PIN diodes to achieve multiband reconfigurability; however, the large number of switching elements increases design complexity and biasing challenges. Frequency-reconfigurable antennas for IoT, LTE, and Wi-Fi applications are discussed in [14, 15]. A 2×2 reconfigurable antenna using varactor diodes to support 1.78 GHz and 2.15 GHz is reported in [16], though the design suffers from narrow bandwidth and

* Corresponding author: Yogesh Shankar Ghodake (yogeshsghodake26@gmail.com).

a complex biasing network. Extensive use of PIN diodes for frequency reconfiguration is documented in [17–24], including dual-band operation from 3.4 to 3.8 GHz. A compact reconfigurable antenna is outlined in [25], and a two-element array with a varactor diode for combined frequency and pattern reconfigurability over 2.15–2.38 GHz is presented in [26]. More complex designs with higher numbers of PIN and varactor diodes are discussed in [27], where the biasing circuitry has a considerable effect on antenna performance. More PIN diodes mean more individual biases needed, which increases system complexity and can degrade performance. Techniques based on metamaterials are used for improving antenna performance in [28], while some designs have relatively low gain in [29]; this is a common drawback of compact reconfigurable antennas. Many reconfigurable antennas have been reported recently [30–33], but most designs either focus on frequency reconfiguration with small bandwidth or pattern reconfiguration that increases switching complexity. A common problem is that most designs need large quantities of switching elements, complicated biasing networks, or big geometries, thus limiting compactness and practical implementation. The antenna architecture described in [34] uses a geometrically intricate radiating structure, comprising a circular microstrip patch, a complex concentric splitring resonator (CSRR), two concentric rings, a defected ground structure (DGS), and PIN-diode switching elements, which collectively contribute to increased design and fabrication complexity. Research may investigate developing Multiple Input Multiple Output (MIMO) antennas that incorporate hybrid reconfigurability, encompassing frequency, radiation pattern, and polarization agility. The proposed antenna is designated as a hybrid antenna array, since it integrates four independently driven radiating elements with PIN-diode — controlled reconfigurable slots, enabling simultaneous frequency and radiation-pattern reconfiguration within a compact framework. The initial mechanism comprises an independently fed four-port array that enables port-specific excitation and isolation control. The second mechanism features a PIN-diode-based current-path reconfiguration network that dynamically modifies the electrical length and current distribution of the radiating structure. Fusing array-level excitation with element-level switching permits simultaneous frequency and radiation-pattern reconfigurability without increasing the antenna footprint or requiring external phase-shifting networks.

The primary contributions of this work are as follows:

- A compact, independently fed, four-port hybrid antenna architecture enabling frequency and radiation-pattern reconfigurability.
- Concurrent reconfigurability of operating frequency and radiation pattern via PIN-diode switching without modifying feeding configuration.
- Realization of sixteen switching configurations using only four PIN diodes, with five representative operating states selected for detailed analysis due to the antenna's structural symmetry.
- Experimental demonstration of wideband operation covering the upper S-band and lower C-band.
- Reduced switching complexity while maintaining high port isolation and stable radiation characteristics.
- The prototype is implemented on a commercially available low-cost FR4 substrate, providing a practical, cost-effective alternative to designs employing expensive low-loss substrates.

This paper is organized into five sections. Section 2 describes the proposed method for designing a reconfigurable antenna. Section 2.1 presents the configuration of the hybrid antenna array. Section 2.2 explains the steps in design evolution, and Section 2.3 provides information on Diode Circuit Modelling. Section 3 describes how to design a frequency- and pattern-reconfigurable hybrid antenna array. After that, there will be measured results and details about the hardware prototype. Section 4 covers diversity analysis, along with a comparative evaluation of the proposed hybrid antenna array against recent studies, including results and discussions. Section 5 provides final remarks and key insights.

2. THE PROPOSED RECONFIGURABLE HYBRID ANTENNA ARRAY DESIGN METHODOLOGY

2.1. Hybrid Antenna Array Configuration

The prototype is fabricated on a 1.6-mm-thick FR-4 epoxy substrate with a relative permittivity (ε_r) of 4.4 and a dielectric loss tangent ($\tan\delta$) of 0.02. Figure 1 shows the design geometry of the four-port, independently fed, reconfigurable microstrip antenna array. It has four lumped-excitation ports, where $W1$ is the feedline width used to excite the elements. Incorporating four PIN diodes (D1–D4) in the radiating slots achieves frequency and radiation pattern reconfigurability. By turning diodes on or off, the effective surface-current path is changed, resulting in different resonant frequencies and radiation patterns for each switching configuration. Impedance matching to a $50\,\Omega$ feedline is obtained by optimizing the distance between the feedline and ground plane. The proposed 2×2 hybrid antenna array is designed on a compact substrate, and its initial dimensions are calculated using standard transmission-line model equations.

$$\text{Width} = \frac{c}{2f_r}\sqrt{\frac{2}{\varepsilon_r+1}} \tag{1}$$

$$\varepsilon_{\mathit{eff}} = \frac{\varepsilon_r+1}{2} + \frac{\varepsilon_r-1}{2}\left(1+12\frac{h}{W}\right)^{-\frac{1}{2}} \tag{2}$$

$$\Delta L = 0.412h\frac{(\varepsilon_{\mathit{eff}}+0.3)\left(\frac{W}{h}+0.264\right)}{(\varepsilon_{\mathit{eff}}-0.258)\left(\frac{W}{h}+0.8\right)} \tag{3}$$

$$\text{Length} = \frac{c}{2f_r\sqrt{\varepsilon_{\mathit{eff}}}} - 2\Delta L, \tag{4}$$

While conventional 2×2 antenna arrays require larger substrate areas or additional decoupling structures, this design achieves a significantly smaller size with good impedance matching and wide bandwidth. The traditional approach often uses defected

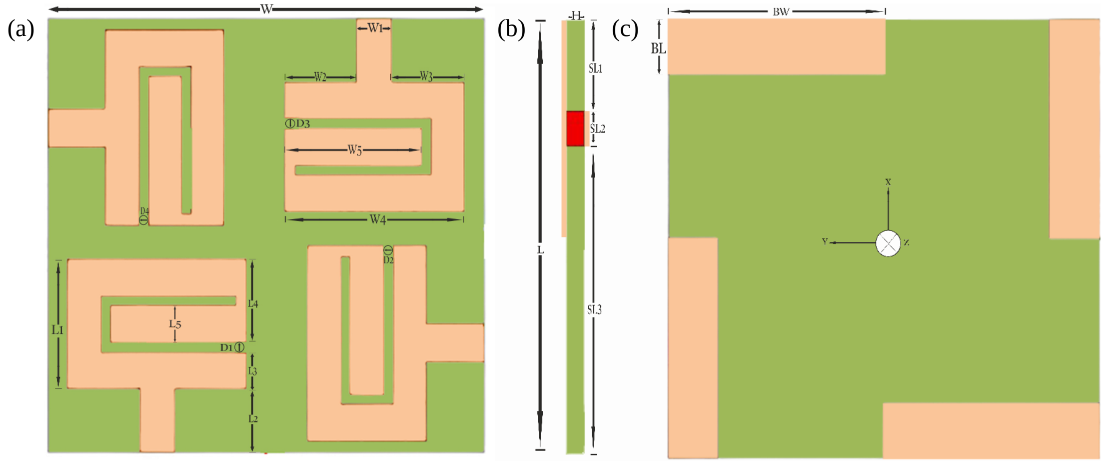

FIGURE 1. The proposed Hybrid Antenna Array geometry. (a) Front view, (b) side view, and (c) back view.

ground structures, increased spacing between elements, or parasitic elements to reduce mutual coupling. These methods increase design complexity and physical size. In contrast, the optimized slot dimensions ($SL1$ and $SL2$) and the uniquely shaped patch geometry in this design allow coupling suppression and improved radiation efficiency without external decoupling networks. The upper copper layer shows four microstrip patches in a top view; the side view gives information about the substrate height, and there is a continuous ground plane on the lower copper layer. The total width and length of the antenna are $40 \times 44\,\mathrm{mm}^2$, which means it has a small size, good for use in portable devices as well as wireless applications built into other devices. Patch sizes ($L1$–$L5$ and $W1$–$W5$) are set to enable both main and higher-order modes so that multi-band operation can happen. Table 1 lists the final optimized geometric parameters from many simulations.

TABLE 1. Dimensions of the proposed hybrid antenna array.

Parameter	Dimension (mm)	Parameter	Dimension (mm)
L	40	W	44
$L1$	12	$W1$	3.5
$L2$	5.8	$W2$	7.2
$L3$	3.83	$W3$	7.3
$L4$	7.66	$W4$	18
$L5$	3.33	$W5$	13.67
BL	5	BW	22
H	1.6	$SL1$	8.3
$SL2$	28.2		

2.2. Evolution Steps

The antenna was examined employing the finite element method (FEM) implemented in Ansys High Frequency Structure Simulator (HFSS). An adaptive meshing algorithm was used until the S-parameters converged. Radiation boundaries were defined around the computational domain, and wave ports were used to excite each antenna port. ON and OFF states of the PIN diode were represented by their equivalent RLC circuits in accordance with the manufacturer's specifications. The antenna design has been taken through five optimization steps, and each step has shown improvement in impedance matching. This is also reflected by the S-parameter levels becoming less positive (or more negative return-loss values) at every step. The first step is a reference design with the initial geometric dimensions and nominal feed placement. This step shows the highest reflection coefficient, meaning that impedance matching is not good here. Steps two and three involve some preliminary geometric changes and adjustments to the feed position; they lead to a moderate improvement in return loss and the beginning of some resonant actions. In Step four, more structural changes, including dimension tuning and adding slots or parasitic elements, greatly improve impedance matching by achieving deeper return-loss minima across the operating band. Step five involves further detailed optimization of patch dimensions, gaps between elements, and feedline parameters that result in clearly defined resonant modes with the lowest reflections found so far at any stage. The last optimized configuration shows a substantial difference in return-loss performance compared to earlier stages, which proves that this iterative design method works well. It means that this antenna is on its way to being very close to perfectly matched; hence, it validates that the proposed hybrid antenna array with partially grounded technique is good for high-efficiency, multi-band operation. Figure 2(a) shows stages of the design evolution, and Figure 2(b) shows corresponding S_{11} characteristics.

2.3. Diode Circuit Modelling

The reconfigurable functionality of the proposed antenna is realized using four BAR6303WE6327HTSA1 PIN diodes obtained from a commercial source. Diodes are actuated via a dedicated DC biasing network powered by a 1.5 V supply and operated in accordance with the manufacturer's recommended forward-bias conditions. The biasing network was designed with compact bias lines and suitable radio frequency (RF) isolation to minimize its impact on the antenna impedance match-

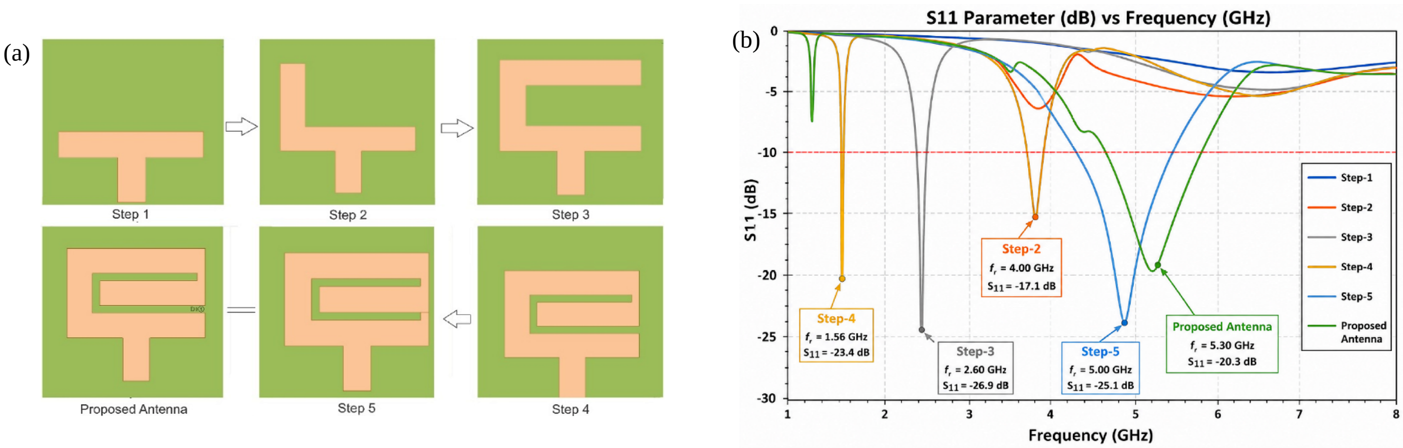

FIGURE 2. (a) Evolution stages of the suggested hybrid antenna array and (b) S_{11} spectra of the various stages.

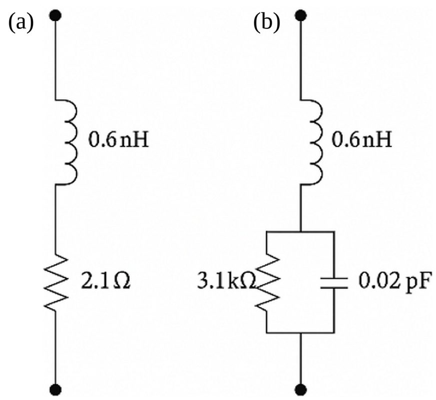

FIGURE 3. The equivalent circuit for the PIN diode is (a) forward-biased and (b) reverse-biased.

ing and radiation characteristics. In ANSYS HFSS simulations, each PIN diode was modeled by an equivalent lumped-element circuit reflecting the device's electrical properties. The ON-state was represented by a series resistance of 2.1 Ω and an inductance of 0.6 nH, while the OFF-state corresponded to a resistance of 3 kΩ, an inductance of 0.6 nH, and a junction capacitance of 0.02 pF; the equivalent circuit for the PIN diode for on and off is depicted in Figure 3. Same commercially available PIN diodes were used in the fabricated prototype to ensure consistency between the simulation model and experimental implementation. The strong agreement between the simulated and measured S-parameters and radiation characteristics confirms the suitability of the chosen PIN diode model and the proposed biasing network for achieving reliable frequency and radiation-pattern reconfigurability.

3. DESIGN APPROACH FOR FREQUENCY AND PATTERN RECONFIGURABLE HYBRID ANTENNA ARRAY

Figure 5 presents the experimental arrangement, and Figure 4 shows fabricated top and ground-plane views of the hybrid antenna array. The antenna's impedance and isolation characteristics were assessed with a vector network analyser over a frequency range from 1 GHz to 8 GHz. The fabricated antenna prototype was characterized using a Rohde & Schwarz Vector Network Analyzer (VNA) with a frequency range of 9 kHz to 13.6 GHz and a characteristic impedance of 50 Ω. Before measurement, a complete two-port Short-Open-Load-Through (SOLT) calibration was performed across the frequency range of interest to eliminate systematic errors attributable to measurement cables and connectors. The VNA was configured with an appropriate frequency span and sweep resolution to accurately capture the antenna's reflection characteristics. Given that a two-port VNA was employed to characterize the four-port independently fed antenna array, the required S-parameters were measured sequentially. During each measurement, the unused antenna ports were terminated with 50 Ω matched loads to emulate operating conditions and minimize reflections, ensuring an accurate evaluation of the antenna's impedance matching and mutual coupling characteristics. The antenna design enables sixteen switching configurations via four PIN diodes. Due to the antenna's structural symmetry, multiple configurations show comparable electromagnetic properties. Consequently, five representative switching configurations, chosen to encompass the antenna's distinct operating behaviours, are selected for in-depth analysis and discussion.

3.1. Frequency Reconfigurability

The frequency-reconfigurable capability of the proposed independently fed, hybrid antenna array is realized by modulating the effective electrical length of radiating elements via PIN-diode switching. By changing the ON/OFF states of the embedded diodes, the surface current paths are reconfigured, yielding distinct resonant frequencies without altering the antenna's physical geometry. To rigorously validate this behaviour, the frequency response of the proposed antenna was examined for each switching state. For each state, the deepest resonant frequencies were determined from the minima of corresponding reflection coefficients (S_{11}, S_{22}, S_{33}, S_{44}), and the associated voltage standing wave ratio (VSWR) values were assessed at the same frequency points. Although isolation between ports is less than -18 to -20 dB, this systematic procedure ensures consistency and minimizes result bias.

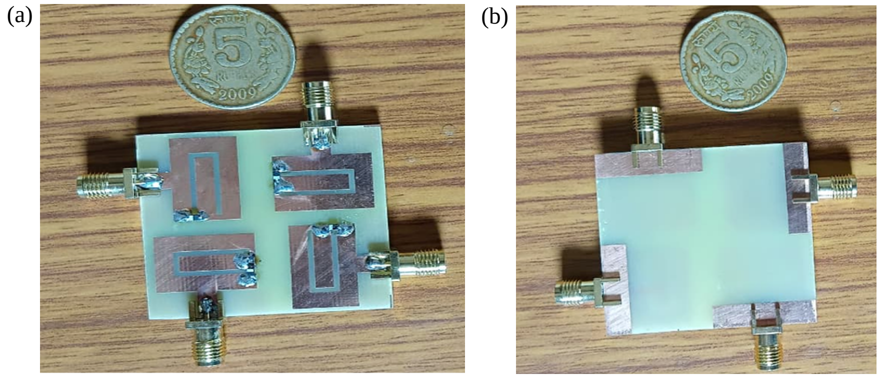

FIGURE 4. Prototype of the proposed Hybrid Antenna Array. (a) Front view and (b) back view.

FIGURE 5. VNA interfaced with the antenna.

3.2. Far-Field Pattern Reconfigurability

The antenna also shows clear radiation pattern reconfigurability via PIN diode switching. Different switching configurations create different radiation behaviours, such as a reference directional pattern, a beam-steered directional pattern, and a directional pattern with shifted main-lobe radiation modes without any physical modification of the antenna structure. These variations are due to state-dependent redistribution of surface currents and excitation asymmetry across radiating elements that allow dynamic control over main-lobe direction, beam shape, and null positions. The transition from symmetric dual-lobe radiation (0000) to directed single-lobe operation (1111), with intermediate beam steering and diagonal coverage states, further confirms effective spatial adaptability. Overall, the proposed antenna achieves both wide frequency tunability and pattern agility in a compact, low-complexity design, making it suitable for adaptive, multi-mode wireless systems operating in sub-6 GHz, C-band, and other spectrum- and space-aware communication platforms.

3.2.1. Total Efficiency vs Frequency

The total efficiency of the proposed antenna at the 0000-switching configuration is calculated using the relationship between realized gain and directivity at the respective resonant frequencies. Total efficiency (ηt) is defined as the ratio of realized gain to directivity in linear scale and can be expressed as follows:

$$\eta t = \frac{Gr}{D} \tag{5}$$

Here, Gr is the realized gain, and D is the antenna directivity. Both these values are taken from full-wave simulation results at their respective frequency points. The gain and directivity obtained in dBi are converted to a linear scale using $10 \sim ((x/10))$ first, and then efficiency is calculated. For the 0000-switching configuration, realized gain and directivity at resonant frequencies 3.8 GHz and 6.2 GHz are 0.3 dBi and 1.7 dBi, respectively. Linear scale conversion gives $Gr \approx 1.07$ and $D \approx 1.48$ for these values; putting them into the above equation gives a total efficiency of about 73.36 percent in contrast. The switching configurations 0000, 0010, and 1000 achieve overall efficiencies of 73.36%, 73.83%, and 73.30% at resonant frequencies of 3.80 GHz, 3.80 GHz, and 3.82 GHz, respectively, indicating effective impedance matching and stable radiation performance. By contrast, states 1111 and 0100 resonate at 4.70 GHz and 4.75 GHz, showing total efficiencies of 25.31% and 23.80%, respectively, due to reduced realized gain relative to directivity under these switching configurations. Overall, the proposed PIN-diode switching mechanism enables frequency reconfigurability across the 3.80–4.75 GHz range by altering

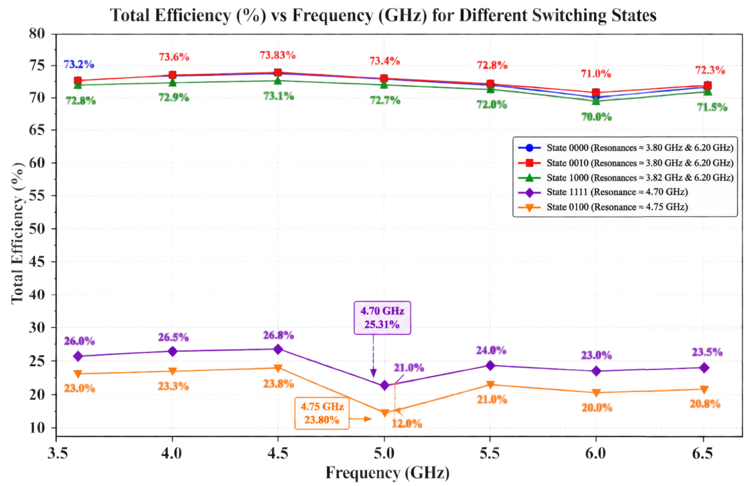

FIGURE 6. Total efficiency vs frequency for states 0000, 0010, 1000, 0100, and 1111.

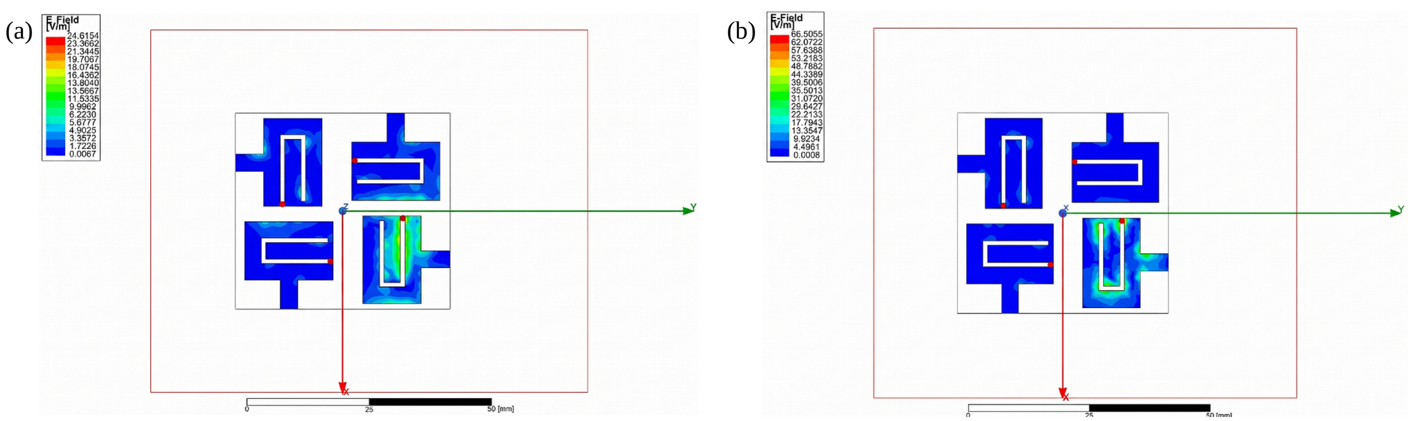

FIGURE 7. Surface current distribution. (a) State 0000 frequency 3.8 GHz and (b) state 1111 frequency 4.7 GHz.

the radiator's effective electrical length while maintaining acceptable radiation performance for the representative operating states, and Figure 6 depicts the total efficiency versus frequency for different switching states.

3.2.2. Surface Current Distribution Analysis

The surface current distributions of the proposed antenna are analysed for 0000 and 1111 switching configurations at their respective resonant frequencies (3.8 GHz and 4.7 GHz) to elucidate the physical mechanism underlying frequency and pattern reconfigurability. In the 0000 state, with all PIN diodes in OFF condition, surface currents follow extended pathways along the radiating slots and patch edges. These extended current trajectories increase the antenna's effective electrical length, yielding lower resonant frequencies and a reference directional radiation pattern. The current distribution exhibits notable asymmetry, accounting for the emergence of dual tilted radiation lobes in the corresponding pattern. Conversely, in the 1111 state, all PIN diodes are switched ON, establishing conductive continuity across reconfigurable slots. Consequently, surface currents become more uniformly distributed and confined to shorter paths over the radiating elements. This reduction in effective electrical length shifts the resonance to higher frequencies and enhances phase coherence across the antenna aperture, resulting in a more directive radiation pattern. The clear difference between these states shows that PIN diode switching changes the current directly, which in turn controls frequency tuning and radiation features, as seen in Figure 7.

4. RESULTS AND DISCUSSION

Using objective selection criteria, namely strong impedance matching ($S_{ii} \leq -15$ dB), low VSWR (≤ 2), isolation ($S_{ij} \leq -18$–20 dB), and multi-band operation, five representative diode states (0110, 0111, 0011, 1111, and 0010) were chosen for detailed discussion. Figure 8 presents a comparison of S_{11} for these states. The results indicate that each diode configuration excites distinct resonant modes across the mid-band (approximately 3.8–4.8 GHz) and the upper band (approximately 5.2–6.46 GHz), demonstrating effective frequency agility.

Simulated resonant frequencies are determined from minimum reflection coefficients (S_{11}, S_{22}, S_{33}, S_{44}) that descend below -10 dB for each switching configuration. The antenna has multiple resonances within the lower (approximately

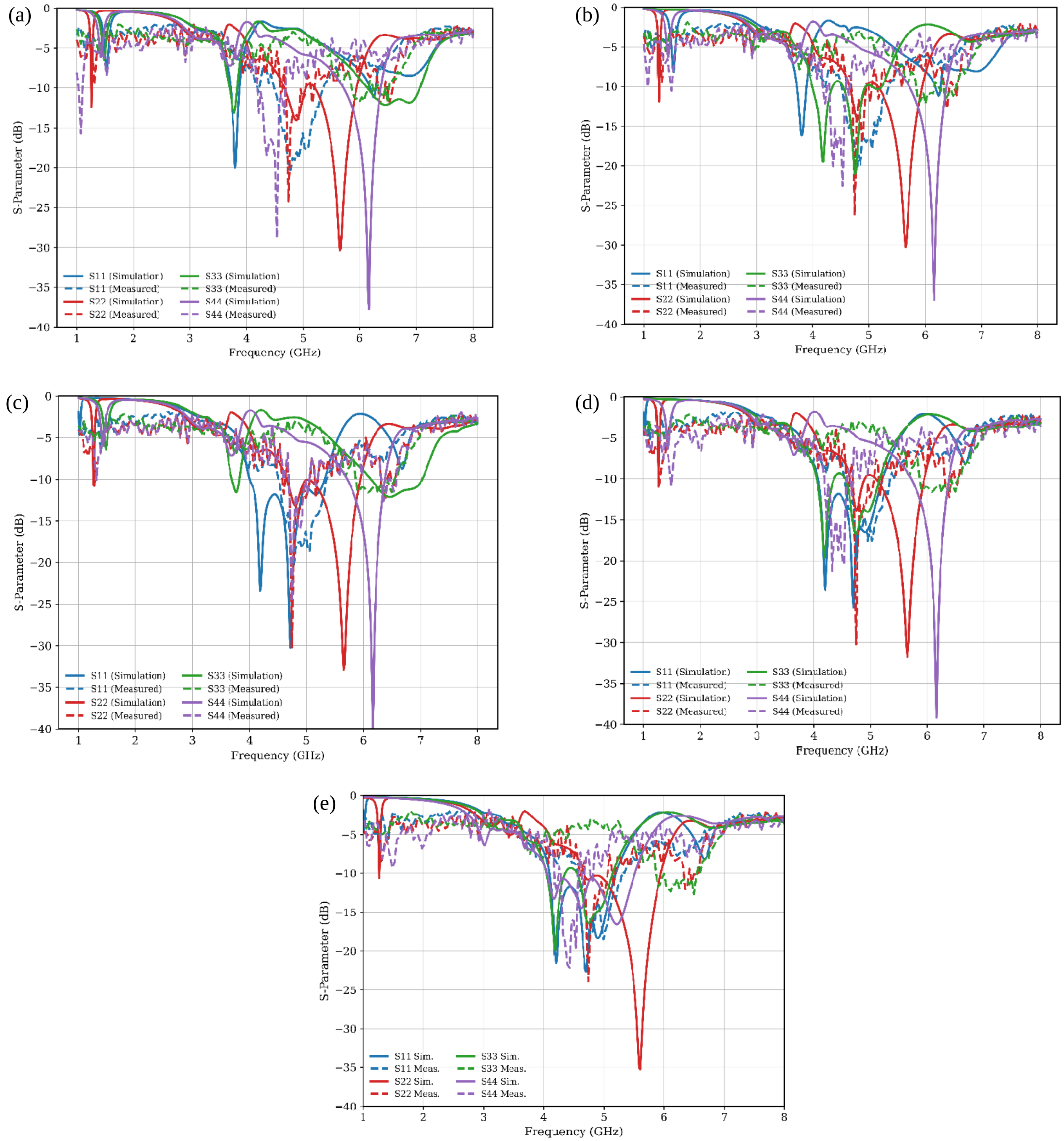

FIGURE 8. Simulated and measured results of the antenna array for State (a) 0010, (b) 0011, (c) 0110, (d) 0111, and (e) 1111.

3.8 GHz), middle (approximately 4.2–4.7 GHz), and upper (approximately 5.6–6.4 GHz) bands, as detailed in Table 2. The shift in resonant frequencies across different diode configurations corroborates effective frequency reconfigurability. Furthermore, strong impedance matching is observed in several states, with reflection coefficients below -30 dB, indicating favourable antenna performance.

Resonant frequencies were determined from minimum reflection coefficients (S_{11}, S_{22}, S_{33}, S_{44}) measured below -10 dB for each switching configuration. The antenna has multiband operation in the lower, middle, and upper frequency ranges, as shown in Table 3. The measured results indicate good impedance matching, with a few reflection coefficients below -35 dB and up to -45 dB. Small frequency shifts compared to the simulated results do not change the general features of frequency reconfigurability; these differences are due to fabrication tolerances, substrate variations, and parasitic effects introduced by the measurement setup and switching elements.

The proposed four-port hybrid antenna attains frequency reconfigurability via independent control of four PIN diodes integrated into the radiating structure. Switching PIN diodes ON or OFF alters the surface-current distribution and the antenna's effective electrical length, yielding different resonant frequencies while maintaining satisfactory impedance

TABLE 2. Application mapping for reconfigurable frequency bands of simulated results.

State	S_{11} (GHz/dB)	S_{22} (GHz/dB)	S_{33} (GHz/dB)	S_{44} (GHz/dB)
0010	$3.80/-20.02$	$5.65/-30.35$	$3.78/-13.11$	$6.27/-37.78$
0011	$3.80/-16.20$	$5.65/-30.27$	$4.75/-21.03$	$6.16/-36.91$
0110	$4.30/-26.30$	$5.65/-32.90$	$6.46/-12.11$	$6.16/-40.75$
0111	$4.70/-25.70$	$5.65/-31.76$	$4.19/-19.61$	$6.16/-39.14$
1111	$4.70/-22.68$	$5.60/-35.26$	$4.19/-19.89$	$5.22/-16.57$

TABLE 3. Application mapping for reconfigurable frequency bands of measured results.

State	S_{11} (GHz/dB)	S_{22} (GHz/dB)	S_{33} (GHz/dB)	S_{44} (GHz/dB)
0010	$4.780/-20.31$	$4.745/-24.20$	$6.495/-11.78$	$4.535/-28.86$
0011	$4.780/-20.60$	$4.745/-26.26$	$6.005/-12.15$	$4.535/-22.56$
0110	$4.745/-20.50$	$4.745/-30.21$	$6.250/-11.75$	$4.745/-24.66$
0111	$4.745/-19.94$	$4.745/-30.21$	$6.250/-11.75$	$4.325/-21.23$
1111	$4.745/-18.65$	$4.745/-23.89$	$6.495/-12.72$	$4.430/-22.20$

matching. The measured and simulated S-parameter responses for representative switching configurations corroborate the antenna's frequency-switching capability. Measured data show that the 0010 state resonates at 4.780 GHz for Port 1 (S_{11}) with a reflection coefficient of -20.31 dB, while Ports 2, 3, and 4 resonate at 4.745 GHz (-24.20 dB), 6.495 GHz (-11.78 dB), and 4.535 GHz (-28.86 dB), respectively. This switching configuration delivers excellent impedance matching across all ports, indicating that activating a single PIN diode effectively alters the current distribution while preserving multi-port operation. In the 0011 state, the antenna preserves its primary resonance at 4.780 GHz for Port 1 with a measured return loss of -20.60 dB. Ports 2, 3, and 4 resonate at 4.745 GHz (-26.26 dB), 6.005 GHz (-12.15 dB), and 4.535 GHz (-22.56 dB), respectively. Compared with the 0010 state, this configuration shows improved matching at Port 2 and a slight shift in Port 3's resonance due to modified surface-current pathways resulting from the additional activated PIN diode. For the 0110 state, the measured resonance shifts to 4.745 GHz for Ports 1 and 2, with reflection coefficients of -20.50 dB and -30.21 dB, respectively. Port 3 resonates at 6.250 GHz (-11.75 dB), and Port 4 at 4.745 GHz (-24.66 dB). Activating additional PIN diodes shortens the antenna's effective electrical length, producing a higher-frequency resonant mode while preserving excellent impedance matching. Similarly, 0111 state yields resonances at 4.745 GHz (-19.94 dB) and 4.745 GHz (-30.21 dB) for Ports 1 and 2, 6.250 GHz (-11.75 dB) for Port 3, and 4.325 GHz (-21.23 dB) for Port 4. Although Ports 1 and 2 retain their resonant frequencies relative to the 0110 state, Port 4 shifts to a lower frequency due to the added conducting path, redistributing the surface currents while maintaining stable impedance characteristics. In the 1111 state, with all PIN diodes forward-biased, measured resonant frequencies are 4.745 GHz (-18.65 dB), 4.745 GHz (-23.89 dB), 6.495 GHz (-12.72 dB), and 4.430 GHz (-22.20 dB) for Ports 1–4, respectively. This configuration corresponds to a fully connected current path, yielding stable multi-port resonance with satisfactory impedance matching across all ports; Figure 8 depicts simulated and measured graphs. Figure 9 shows measured adjacent-port isolation characteristics for the proposed independently fed four-port antenna for representative switching configurations 0000 and 1111 in Figures 9(a) and (b), respectively. Results indicate satisfactory inter-port isolation across the operating frequency range, with isolation typically better than -18 to -20 dB and reaching approximately -40 dB to -50 dB at several resonant frequencies. The optimized antenna geometry on the FR4 substrate, in conjunction with the PIN diode switching network, effectively governs surface-current distribution while preserving low mutual coupling during reconfiguration. These findings confirm that the proposed antenna maintains stable isolation while enabling both frequency and radiation-pattern reconfigurability for wireless communication applications. The measured adjacent-port isolation for the other representative switching configurations (0010, 0011, 0110, and 0111) shows comparable isolation behaviour and follows the same overall trend. Consequently, to avoid repetition across figures and enhance manuscript clarity, only the measured isolation results for the representative switching configurations 0000 and 1111 are presented.

Overall, measurements demonstrate that the proposed antenna achieves frequency reconfigurability via PIN diode switching. The resonant frequencies span approximately 4.325 GHz to 6.495 GHz, depending on the switching configuration and excited port. The measured results align well with simulations, confirming that the switching network effectively governs the antenna's electrical length and current distribution without compromising impedance performance.

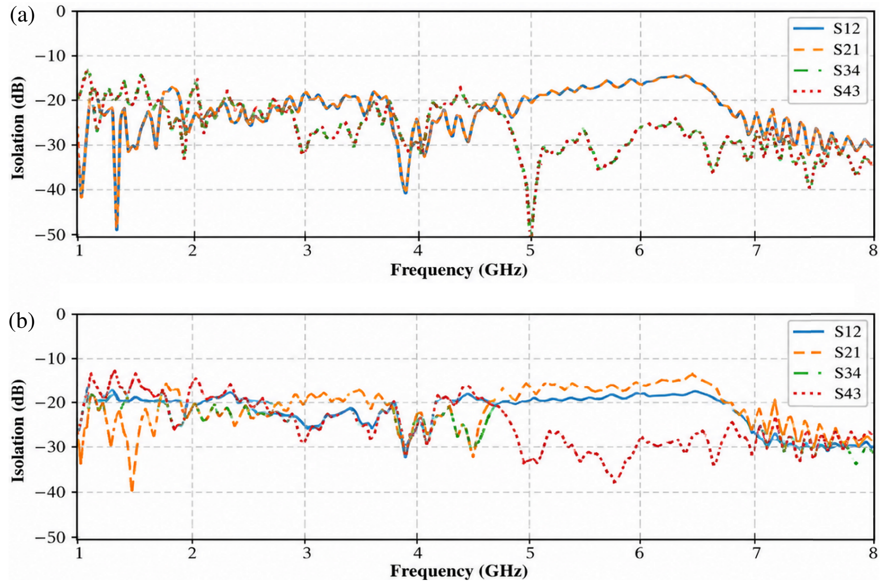

FIGURE 9. Isolation characteristics of four-port states 0000 and 1111. (a) Measured adjacent-port isolation characteristics of the proposed four-port antenna for switching state 0000 and (b) measured adjacent-port isolation characteristics of the proposed four-port antenna for switching state 1111.

Consequently, the antenna supports reliable multi-frequency operation suitable for adaptive sub-6 GHz wireless systems, including 5G, WLAN, WiMAX, and other contemporary applications.

The radiation-pattern reconfigurability of the proposed hybrid antenna array is achieved by the ON/OFF switching of integrated PIN diodes, effectively changing the electrical continuity of the radiating structure. For all simulated radiation characteristics, only Port 1 was excited with an input power 1 W and a phase 0°, while the remaining three ports were assigned 0 W excitation during post-processing in ANSYS HFSS. Excitation conditions were kept identical for all simulations, and only PIN diode switching configurations were varied. Therefore, the observed changes in the radiation patterns are solely attributed to the reconfiguration introduced by the PIN diode switching network. Figures 10(a)–(e) show corresponding simulated radiation patterns for some selected switching configurations; green and red curves represent principal-plane components and clearly indicate state-dependent changes in beam shape, orientation, and null locations. In the 0000-switching configuration, all PIN diodes are OFF, resulting in high-impedance discontinuities across the reconfigurable slots. This forces surface current to take longer asymmetric paths along patch edges and slot boundaries. The phase imbalance between radiating sections causes constructive interference at off-broadside angles and destructive interference along the normal axis. Therefore, a bidirectional radiation pattern with two dominant lobes tilted symmetrically at about $\pm 60^\circ$ can be seen from the green and red curves in Figure 10(a); this state is the default for antenna radiation mode. When all PIN diodes are turned ON (1111 state), conductive continuity is established through the slots, thereby significantly reducing effective current paths and increasing phase coherence over the aperture. ON-state diodes act as low-impedance paths so that the current magnitude is uniform with almost equal phase excitation for all main radiating sections; thus, far-field radiation will be dominated by constructive interference in one angular direction, resulting in a unidirectional pattern with a strong main lobe and low back radiation, as shown in Figure 10(b). The better alignment of these two curves (green and red) means more directivity and a higher front-to-back ratio than those with 0000.

In intermediate switching configurations, symmetric diode activation creates an asymmetrical current distribution in a controlled manner. In the 1000 state with only one diode ON, it creates a low-impedance path on one side of the antenna, which means that more current will flow with phase advancement into that area while all other OFF-state diodes keep their corresponding regions discontinuous. As per array radiation theory, the far-field pattern changes subsequently in a state-dependent manner.

$$E(\theta) = \sum_{n=1}^{N} I_n e^{j(\beta r_n \cos\theta + \psi_n)} \tag{6}$$

The radiation pattern is now controlled by unequal phase terms (ψ_n), which change the condition for constructive interference. As a result, the main radiation lobe is directed toward a certain angular sector (around $+60^\circ$) with a smaller back lobe, as seen in Figure 10(c). This proves that electronic beam steering can be achieved via current redistribution.

In the 0100 state, the diode that is turned on is located on the opposite side of the antenna in the 1000 state. Even though the physical shape does not change, the position of the conductive path flips the asymmetry of surface current and the phase gradient across the aperture. Therefore, it produces a mirrored response to radiation with its main lobe pointing towards an opposite angular region, as shown in Figure 10(d). The green-red lobe, which was previously dominant, now points in another direction, proving that beams can be reversed and thus allowing coverage to adapt in two different spatial directions. In the 0010 state, turning on this diode creates a current path that is

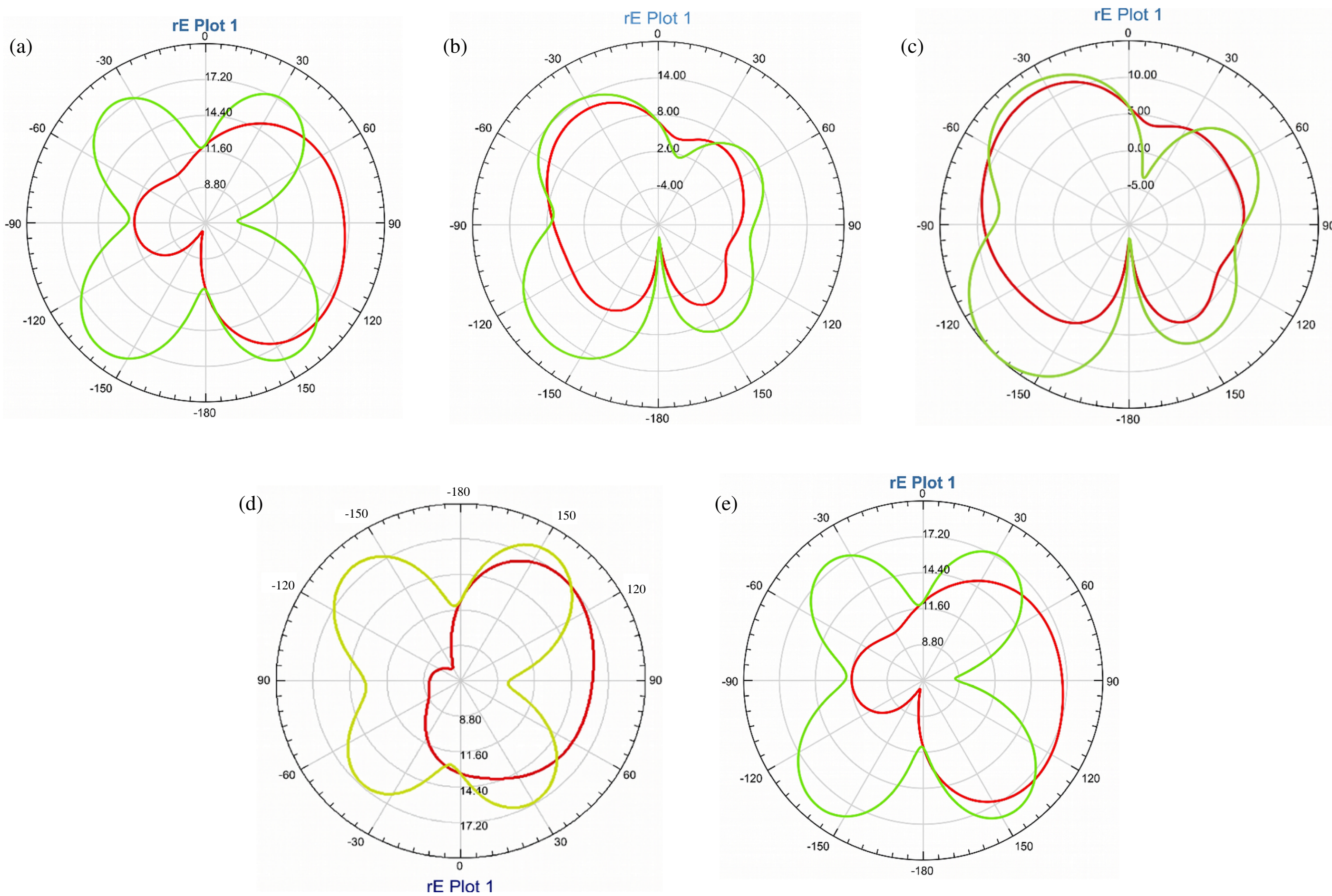

FIGURE 10. Radiation pattern reconfigurability at resonant frequency. (a) State: 0000, (b) State: 1111, (c) State: 1000, (d) State: 0100, and (e) State: 0010.

not purely symmetric and not aligned with any principal axis. The surface current takes a diagonal path, which brings about simultaneous phase gradients in both orthogonal directions. A diagonal radiation pattern results from this condition; it shows stronger emission toward one diagonal quadrant and has an especially deep null around $-180°$ (see Figure 10(e)). The difference between these two curves indicates that non-orthogonal radiation modes are forming here — modes better suited for diagonal or sectorized coverage. Collectively, the progression from reference directional pattern (0000) to beam-steered directional pattern (1111), directional pattern with shifted main lobe (1000), tilted directional pattern (0100), and diagonally oriented (0010) radiation patterns demonstrates that PIN-diode controlled redistribution of surface current directly governs the antenna's radiation behaviour. Crucially, these pattern transformations are achieved without any physical modification to the antenna structure, relying exclusively on electronic switching. This substantiates the proposed design as a compact, versatile, pattern-reconfigurable antenna capable of dynamic spatial adaptation for contemporary wireless communication systems. Table 4 details the radiation pattern with the above states, 0000, 1111, 1000, 0100, and 0010, along with their corresponding frequency, bandwidth, and pattern modes. The impedance bandwidth of the structured prototype is determined using the -10 dB return-loss criterion, where the lower (f_L) and upper (f_H) cutoff frequencies correspond to the frequencies at which the reflection coefficient crosses -10 dB. The absolute bandwidth (BW) is calculated as

$$\text{BW} = f_H - f_L \tag{7}$$

The fractional bandwidth (FBW) is then calculated using the center frequency (f_c) as

$$\text{FBW}\,(\%) = \frac{f_H - f_L}{f_c} \times 100, \tag{8}$$

and

$$f_c = \frac{f_H + f_L}{2} \tag{9}$$

Using this approach, the calculated fractional bandwidths for representative switching configurations are 51.05%, 23.66%, 50.55%, 27.84%, and 51.05%, respectively.

Figure 11 displays simulated and measured S-parameter characteristics of the proposed four-port, frequency-tunable antenna for representative switching configurations (0000, 0010, 0011, 0110, and 1111). The solid and dashed curves denote the simulated and measured results, respectively, illustrating

TABLE 4. Pattern reconfigurability (from radiation plots).

Switch State	Resonant Frequency (GHz)	Bandwidth (GHz)	Bandwidth (%)	Peak Realized Gain (dBi)	Peak Directivity (dBi)	Total Efficiency (%)	Observation	Pattern Mode
0000	3.80	2.55	51.05	0.339	1.685	73.36	Two dominant main lobes observed, symmetrically tilted at approximately $\pm 60^\circ$	Reference directional pattern
1111	4.70	1.10	23.66	-1.696	4.272	25.31	Single dominant main lobe formed toward the $+90^\circ$ direction with suppressed back radiation	Directional pattern with shifted main lobe
1000	3.82	2.54	50.55	0.338	1.687	73.30	Main radiation lobe shifts toward approximately $+60^\circ$ with reduced back-lobe level	Directional pattern with shifted main lobe
0100	4.75	1.31	27.84	-2.889	3.346	23.80	Radiation lobe flips toward the opposite angular region compared to state 1000	Tilted directional pattern
0010	3.80	2.55	51.05	0.385	1.702	73.83	Distinct Directional pattern with shifted main lobe tilt with a deep null around -180° and enhanced radiation in the lower-right quadrant	Directional pattern with shifted main lobe

TABLE 5. Comparison of frequency and pattern reconfigurable hybrid antenna array.

Parameter	**[30]**	**[31]**	**[6]**	**[32]**	**[33]**	**[25]**	**[29]**	**[34]**	**Proposed**
Year	2023	2019	2023	2022	2023	2023	2024	2025	**2026**
Size (mm^2)	48×32	200×150	50×25	50×30	100×50	30×26	38×29.4	60×63	$\mathbf{44 \times 40}$
Substrate	Rogers RT/ Duroid 5880	Rogers RO4350	Rogers RT/ Duroid	FR4	FR4	FR4	FR4	FR4	**FR4**
Number of Ports	2	8	2	2	2	2	2	1	**4**
PIN Diode Switches	4	4	4	2	2	4	2	2	**4**
Frequency Reconfigurable	✓	✓	✓	✓	✓	✓	✓	✓	✓
Pattern Reconfigurable	×	×	×	×	×	×	×	×	✓
Isolation (dB)	> 20	> 15	> 20	> 20	> 20	> 20	> 20	NA	$\mathbf{> 18}$ $\mathbf{> 20}$
Peak Gain (dBi)	2.04	NA	2.76	2.47	2.20	2.46	2.00	6.20	**1.0–2.88**
Total Efficiency (%) (State dependent)	NA	NA	NA	NA	NA	NA	NA	NA	**(0000-70.5–73.5) (1111-72.5–79.5)**
Bandwidth (%)	58.1	102.6	200	22.1	84.5	200	NA	11.34–27.95	**23.66–51.05**
Frequency Range (GHz)	3.3–6.0	1.48–4.56	3.2–5.7	3.4–3.8	1.42–2.27	2.4–5.7	S, C & X Bands	5G Sub-6 GHz	**3.7–6.3**
Measured Validation	Yes	Yes	Yes	Yes	Yes	Yes	Yes	Yes	**Yes**

good agreement across all switching configurations. The antenna maintains a reflection coefficient below -10 dB. The impedance bandwidth for each port is determined using the -10 dB return-loss criterion, with lower and upper cut-off frequencies (fL and fH) defined as intersections of the S-parameter curve with the -10 dB reference line.

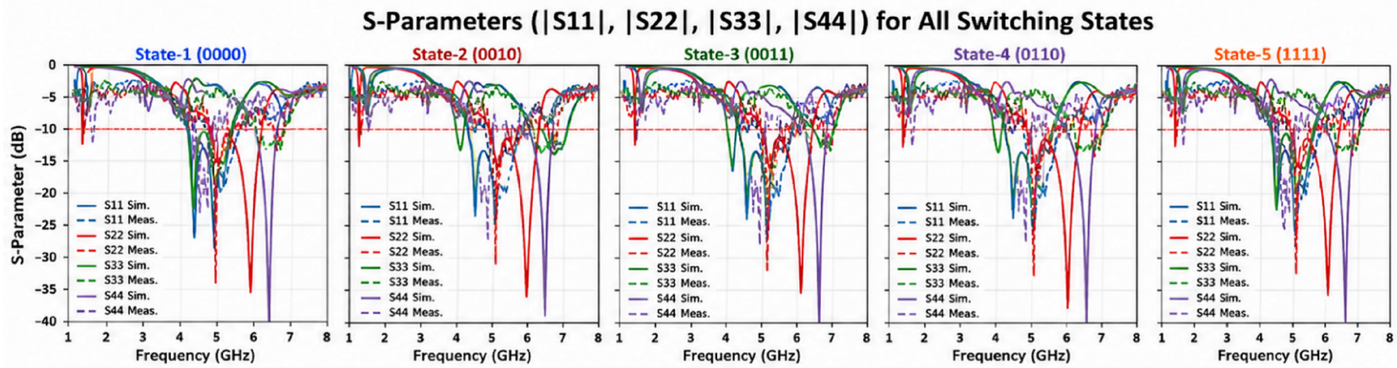

Bandwidth Calculation Method:

- The impedance bandwidth is defined using the −10 dB return loss criterion.
- For each port (S11, S22, S33, S44), the lower (f_L) and upper (f_H) frequencies are determined at the −10 dB points.
- Bandwidth $(BW) = f_H - f_L$
- Fractional Bandwidth $(FBW\%) = \frac{f_H - f_L}{f_c} \times 100$, where $f_c = \frac{f_H + f_L}{2}$

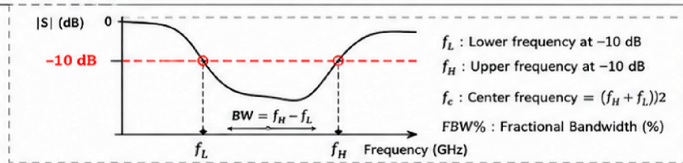

−10 dB Impedance Bandwidth Results

Switching State	Port	Simulation ($\lvert S \rvert \le -10$ dB)					Measurement ($\lvert S \rvert \le -10$ dB)				
		f_L (GHz)	f_H (GHz)	BW (GHz)	f_c (GHz)	FBW (%)	f_L (GHz)	f_H (GHz)	BW (GHz)	f_c (GHz)	FBW (%)
State-1 (0000)	S11	3.72	6.27	2.55	4.99	51.05	4.12	5.45	1.33	4.79	27.76
	S22	3.55	6.81	3.26	5.18	62.93	4.10	6.48	2.38	5.29	45.00
	S33	3.48	7.02	3.54	5.25	67.43	5.40	6.90	1.50	6.15	24.39
	S44	3.82	6.32	2.50	5.07	49.31	4.02	6.62	2.60	5.32	48.87
State-2 (0010)	S11	3.71	6.26	2.55	4.98	51.17	4.15	5.38	1.23	4.77	25.84
	S22	3.62	6.74	3.12	5.18	60.23	4.08	6.51	2.43	5.30	45.85
	S33	3.45	7.05	3.60	5.25	68.62	5.42	6.93	1.51	6.18	24.44
	S44	3.84	6.30	2.46	5.07	48.52	4.02	6.60	2.58	5.31	48.59
State-3 (0011)	S11	3.73	6.24	2.51	4.98	50.40	4.10	5.47	1.37	4.79	28.60
	S22	3.58	6.72	3.14	5.15	60.96	4.05	6.55	2.50	5.30	47.17
	S33	3.88	7.01	3.13	5.45	57.26	5.35	6.85	1.50	6.10	24.59
	S44	3.86	6.28	2.42	5.07	47.73	4.00	6.58	2.58	5.29	48.79
State-4 (0110)	S11	3.86	6.28	2.42	5.07	47.73	4.30	5.62	1.32	4.96	26.61
	S22	3.60	6.70	3.10	5.15	60.19	4.12	6.48	2.36	5.30	44.53
	S33	3.82	7.08	3.26	5.45	59.82	5.38	6.88	1.50	6.13	24.47
	S44	3.88	6.30	2.42	5.09	47.53	4.05	6.60	2.55	5.33	47.82
State-5 (1111)	S11	3.88	6.34	2.46	5.11	48.14	4.20	5.60	1.40	4.90	28.57
	S22	3.62	6.64	3.02	5.13	58.87	4.15	6.45	2.30	5.30	43.40
	S33	3.90	7.03	3.13	5.47	57.15	5.40	6.85	1.45	6.13	23.64
	S44	3.90	6.20	2.30	5.05	45.54	4.20	6.52	2.32	5.36	43.28

FIGURE 11. S-parameter analysis and bandwidth results.

The novelty of this work resides in developing a compact, independently fed hybrid antenna array that attains both wideband frequency reconfigurability and radiation-pattern agility using only four PIN diodes. As summarized in Table 5, the proposed array occupies a compact footprint of $40 \times 44\,\text{mm}^2$ while delivering five distinct switching configurations, substantially reducing switching and biasing complexity compared with many existing reconfigurable designs that rely on a greater number of actuators. The proposed structure is implemented on a commercially available low-cost FR4 substrate, providing a practical, cost-effective alternative to designs based on expensive low-loss substrates. In contrasting with prior approaches that predominantly emphasize either frequency or pattern reconfiguration over narrow bandwidths, the proposed antenna supports continuous operation across the upper S-band and lower C-band (3.7–6.3 GHz) with a -10 dB impedance bandwidth of up to 51.05% for states 0000 and 0010 under simulated results. Moreover, multiple radiation modes — reference directional pattern, beam-steered directional pattern, directional pattern with shifted main lobe, tilted directional pattern, and diagonal patterns — are realized via electronic switching without mechanical motion or additional phase-shifting networks. In sum, the design offers a cost-effective compromise among compactness, bandwidth, and reconfigurability, setting it apart from existing reconfigurable antennas and making it well suited for sub-6 GHz and C-band adaptive RF front-end applications.

5. CONCLUSION

This study introduces a compact, independently fed, PIN diode-based four-port hybrid antenna array that offers simultaneous frequency and radiation-pattern reconfigurability for sub-6 GHz wireless applications. The proposed antenna incorporates four PIN diodes, enabling sixteen switching configurations, with five representative configurations examined in detail. Simulations indicate reconfigurable frequency operation, with resonant frequencies spanning approximately 3.80 to 4.75 GHz and impedance bandwidths of 23.66% to 51.05% for the representative configurations. Radiation-pattern reconfigurability is achieved through beam steering and modifications to the main-lobe characteristics under varying switching configurations, while maintaining satisfactory realized gain, directivity, and total efficiency. The fabricated prototype was experimentally characterized using a calibrated vector network analyzer, and measured S-parameters corroborate the frequency-reconfigurable behavior of the proposed antenna, showing good agreement with simulated results. The experimentally validated performance, in conjunction with the compact four-port architecture, low switching complexity, and low-cost FR4 implementation, demonstrates the practical feasibility of the proposed antenna for adaptive sub-6 GHz wireless communication systems.

REFERENCES

[1] Gupta, M., S. Sharma, H. Joshi, and S. J. Darak, "Reconfigurable architecture for spatial sensing in wideband radio front-end," *IEEE Transactions on Circuits and Systems II: Express Briefs*, Vol. 69, No. 3, 1054–1058, 2022.

[2] Kantemur, A., J. Tak, P. Siyari, A. H. Abdelrahman, M. Krunz, and H. Xin, "A novel compact reconfigurable broadband antenna for cognitive radio applications," *IEEE Transactions on Antennas and Propagation*, Vol. 68, No. 9, 6538–6547, 2020.

[3] Hussain, M., E. M. Ali, W. A. Awan, N. Hussain, M. Alibakhshikenari, B. S. Virdee, and F. Falcone, "Electronically reconfigurable and conformal triband antenna for wireless communications systems and portable devices," *PLoS ONE*, Vol. 17, No. 12, e0276922, 2022.

[4] Chattha, H. T., M. K. Ishfaq, B. A. Khawaja, A. Sharif, and N. Sheriff, "Compact multiport MIMO antenna system for 5G IoT and cellular handheld applications," *IEEE Antennas and Wireless Propagation Letters*, Vol. 20, No. 11, 2136–2140, 2021.

[5] Awan, W. A., N. Hussain, S. A. Naqvi, A. Iqbal, R. Striker, D. Mitra, and B. D. Braaten, "A miniaturized wideband and multi-band on-demand reconfigurable antenna for compact and portable devices," *AEU — International Journal of Electronics and Communications*, Vol. 122, 153266, 2020.

[6] Rathore, P. S., R. Mali, R. Jatav, and M. K. Meshram, "Integrated compact UWB and frequency reconfigurable antenna with high isolation for cognitive radio," *AEU — International Journal of Electronics and Communications*, Vol. 171, 154899, 2023.

[7] Hassan, M. M., Z. Zahid, A. A. Khan, I. Rashid, A. Rauf, M. Maqsood, and F. A. Bhatti, "Two element MIMO antenna with frequency reconfigurable characteristics utilizing RF MEMS for 5G applications," *Journal of Electromagnetic Waves and Applications*, Vol. 34, No. 9, 1210–1224, 2020.

[8] Thanki, P. and F. Raval, "Fork-shaped frequency and pattern reconfigurable antenna," *International Journal of Communication Systems*, Vol. 33, No. 17, e4613, 2020.

[9] Sathikbasha, M. J. and V. Nagarajan, "Design of multiband frequency reconfigurable antenna with defected ground structure for wireless applications," *Wireless Personal Communications*, Vol. 113, No. 2, 867–892, 2020.

[10] Saha, P. B., D. Ghoshal, S. Roy, and R. K. Dash, "Frequency reconfigurable two-element MIMO antenna for 3G/4G/5G cellular communications," in *2021 IEEE Indian Conference on Antennas and Propagation (InCAP)*, 965–968, Jaipur, Rajasthan, India, 2021.

[11] Aldar, D. S., "Frequency selective reconfigurable microstrip antenna for cognitive radio applications," *Advanced Electromagnetics*, Vol. 11, No. 4, 60–68, 2022.

[12] Ahmad, I., W. U. R. Khan, H. Dildar, S. Ullah, S. Ullah, N. Mufti, B. Kamal, T. Ahmad, A. Ghaffar, and M. I. Hussien, "A pentaband compound reconfigurable antenna for 5G and multi-standard sub-6 GHz wireless applications," *Electronics*, Vol. 10, No. 20, 2526, 2021.

[13] Singh, P. P., P. K. Goswami, S. K. Sharma, and G. Goswami, "Frequency reconfigurable multiband antenna for IoT applications in WLAN, WiMAX, and C-band," *Progress In Electromagnetics Research C*, Vol. 102, 149–162, 2020.

[14] Bharadwaj, S. S., D. Sipal, D. Yadav, and S. K. Koul, "A compact tri-band frequency reconfigurable antenna for LTE/Wi-Fi/ITS applications," *Progress In Electromagnetics Research M*, Vol. 91, 59–67, 2020.

[15] Raza, A., M. U. Khan, F. A. Tahir, R. Hussain, and M. S. Sharawi, "A 2-element meandered-line slot-based frequency reconfigurable MIMO antenna system," *Microwave and Optical Technology Letters*, Vol. 60, No. 11, 2794–2801, 2018.

[16] Khan, T. and M. Rahman, "Design of low-profile frequency reconfigurable antenna for multiband applications," *International Journal of Electronics Letters*, Vol. 10, No. 1, 30–47, 2022.

[17] Fakharian, M. M., P. Rezaei, and A. A. Orouji, "A multi-reconfigurable CLL-loaded planar monopole antenna," *Radioengineering*, Vol. 29, No. 2, 313–320, 2020.

[18] Shaw, M. and Y. K. Choukiker, "Frequency reconfigurable microstrip patch antenna for IRNSS applications," in *2020 International Conference on Inventive Computation Technologies (ICICT)*, 878–880, Coimbatore, India, 2020.

[19] Sharma, M., Vikas, and N. Kumar, "Design and analysis of frequency reconfigurable multiband antenna (Bluetooth/downlink frequencies for INSAT/downlink X-band satellite system) using PIN diodes for wireless communication systems," in *2020 IEEE International Conference on Computing, Power and Communication Technologies (GUCON)*, 90–94, Greater Noida, India, 2020.

[20] Iqbal, A., A. Smida, N. K. Mallat, R. Ghayoula, I. Elfergani, J. Rodriguez, and S. Kim, "Frequency and pattern reconfigurable antenna for emerging wireless communication systems," *Electronics*, Vol. 8, No. 4, 407, 2019.

[21] Kumar, J., B. Basu, and F. A. Talukdar, "Modeling of a PIN diode RF switch for reconfigurable antenna application," *Scientia Iranica*, Vol. 26, No. 3, 1714–1723, 2019.

[22] Iqbal, A., A. Smida, L. F. Abdulrazak, O. A. Saraereh, N. K. Mallat, I. Elfergani, and S. Kim, "Low-profile frequency reconfigurable antenna for heterogeneous wireless systems," *Electronics*, Vol. 8, No. 9, 976, 2019.

[23] Shah, I. A., S. Hayat, A. Basir, M. Zada, S. A. A. Shah, and S. Ullah, "Design and analysis of a hexa-band frequency reconfigurable antenna for wireless communication," *AEU — International Journal of Electronics and Communications*, Vol. 98, 80–88, 2019.

[24] Liu, J., J. Li, and R. Xu, "Design of very simple frequency and polarisation reconfigurable antenna with finite ground structure," *Electronics Letters*, Vol. 54, No. 4, 187–188, 2018.

[25] Li, X. and H. Xu, "A compact dual trap reconfigurable ultra-wideband MIMO antenna design," in *2023 4th International Symposium on Computer Engineering and Intelligent Communications (ISCEIC)*, 466–471, Nanjing, China, 2023.

[26] Zainarry, S. N. M., N. Nguyen-Trong, and C. Fumeaux, "A frequency- and pattern-reconfigurable two-element array antenna," *IEEE Antennas and Wireless Propagation Letters*, Vol. 17, No. 4, 617–620, 2018.

[27] Romputtal, A. and C. Phongcharoenpanich, "Frequency reconfigurable multiband antenna with embedded biasing network," *IET Microwaves, Antennas & Propagation*, Vol. 11, No. 10, 1369–1378, 2017.

[28] Chetan, S., D. N. Chandrappa, G. S. Yogesh, S. Jagadeesha, and S. K. Sreedharamurthy, "Design and performance analysis of multiband patch antenna with metamaterial for wireless applications," *Indian Journal of Science and Technology*, Vol. 17, No. 3, 270–276, 2024.

[29] Deshmukh, V. and S. Chorage, "Multifunctional frequency reconfigurable antenna array for future wireless communication," *International Journal of Electronics and Communication Engineering*, Vol. 11, No. 10, 211–226, Oct. 2024.

[30] Saleem, S., S. Kumari, D. Yadav, M. G. Siddiqui, and D. Bhatnagar, "A planar UWB-MIMO antenna with high isolation and reconfigurable single band-elimination characteristics," *AEU — International Journal of Electronics and Communications*, Vol.

170, 154853, 2023.

[31] Hussain, R. and M. S. Sharawi, "An integrated slot-based frequency-agile and UWB multifunction MIMO antenna system," *IEEE Antennas and Wireless Propagation Letters*, Vol. 18, No. 10, 2150–2154, 2019.

[32] Singh, A. K., S. K. Mahto, P. Kumar, R. K. Mistri, and R. Sinha, "Reconfigurable circular patch MIMO antenna for 5G (sub-6 GHz) and WLAN applications," *International Journal of Communication Systems*, Vol. 35, No. 16, e5313, 2022.

[33] Nej, S., A. Ghosh, J. Kumar, and S. Das, "Ultra-wideband MIMO antenna with reconfigurable band notch characteristics and improved isolation," *AEU — International Journal of Electronics and Communications*, Vol. 170, 154849, 2023.

[34] Uchariya, P., P. Ranjan, S. Kumar, *et al.*, "Machine learning assisted frequency reconfigurable concentric split ring resonator inspired antenna for sub-6 GHz 5G and IEEE 802.11 ba/Be applications," *AEU — International Journal of Electronics and Communications*, Vol. 200, 155889, 2025.